Representative Model Compounds for Understanding the Pyrolytic Behavior of Pre-oxidized β-Ether-type Lignin

Shuyun Liu,[a] Weikun Jiang,[a,*] Bo Jin,[b] Yu Liu,[a,*] and Lucian A. Lucia [a]

To achieve a better understanding of the pyrolysis behavior of pre-oxidized β-ether-type lignin, three C_α=O type dimers with different substituent groups on the aromatic ring were synthesized and analyzed by a simultaneous thermal analysis instrument (STA), *in-situ* Fourier transform infrared spectroscopy (*in-situ* FTIR), and pyrolysis-gas chromatography/ mass spectrometry (Py-GC/MS). The results showed that major primary pyrolysis reactions of C_α=O type models normally occurred at 200 to 400 °C, and connecting bridge structures of models were completely destroyed, causing the emission of abundant volatiles. Substituent groups of aromatic rings played direct roles in thermal stability of models, volatiles emission, product characteristics, and secondary reaction pathways of major primary products. Particularly, the aryl–OCH_3 group clearly enhanced the reactivity of intramolecular linkages and was an important active functional group for secondary reactions. As major primary products and intermediates, guaiacol and 2-methoxy-benzaldehyde were formed *via* the cleavage of C_α–O and C_α–C_β bonds and could also be converted into phenol, benzaldehyde, and 2-methylphenol *via* rearrangement of aryl–OCH_3 into an aryl–CH_3 group or –OCH_3 group removal. Oxidization of benzylic alcohol to benzylic ketone not only simplified depolymerization pathways, but also resulted in better selectivity of phenolic monomers and a predictable product distribution.

Keywords: Pre-oxidized lignin models; Pyrolysis behavior; Substituent groups; in-situ FTIR

*Contact information: a: State Key Laboratory of Biobased Material and Green Papermaking College of Paper and Plant Resources Engineering, Qilu University of Technology, Jinan, Shandong 250353, PR China; b: School of Chemistry and Chemical Engineering, Shandong University, Jinan, Shandong 250100, PR China; *Corresponding authors: weikun0709@126.com; leoliuyu@163.com*

INTRODUCTION

Although oil refinery operations are the main source of chemicals in society today, a worldwide energy crisis and environmental concerns dictate consideration of alternative feedstock for chemicals such as renewables (Ralph *et al*. 2019). Lignocellulosic biomass is the only renewable organic carbon resource in nature, and it is mainly composed of hemicelluloses, cellulose, and lignin. For hemicellulose and cellulose, several mature utilization technologies have been adopted industrially for the production of biofuels and platform chemicals (Chen and Kuo 2011). Lignin, the most abundant and renewable source composed of aromatic units in nature, is quite valuable for producing value-added aromatic chemicals. Annually, millions of tons of alkali-soluble lignin and solid residue lignin are produced by the pulp and paper industry and bioethanol industry (No 2014; Farag and Chaouki 2015; Ong *et al*. 2019). Selective abstraction of desired aromatic and phenolic products from lignin should have constituted a renewable resource for these valuable

chemicals. However, due to lignin's complexity and structural variety, all but a small percentage of the lignin is used in low-value commercial applications, such as fuel for heat and power applications (Han *et al*. 2018).

A representative lignin structure is illustrated in Fig. S1a (see Apptendix), and all these monomeric units contain a phenyl nuclei and a propyl side chain. Lignin is mainly composed of three primary precursors: sinapyl (S), coniferyl (G), and p-coumaryl (H) alcohols; these are linked by ether linkages (*e.g.*, β–O–4 and α–O–4) and carbon-carbon linkages (*e.g.*, 5–5 and β–1 linkages) (Boerjan *et al*. 2003; Crestini *et al*. 2017). Theoretically, by breaking down these linkages, particularly the β–O–4 bonds, which are the predominant linkage in lignin, a lot of high added value phenolic chemicals, such as benzene, phenol, guaiacol, vanillin, acetovanillone, and their derivates, could be obtained. Over the last few decades, a number of strategies (Li *et al.* 2015, Ong *et al.* 2019), such as pyrolysis, hydrogenolysis, hydrolysis, and enzymatic reactions, have been undertaken to depolymerize lignin. Among them, the most traditional lignin depolymerization strategy is pyrolysis, the rapid thermal decomposition at approximately 500 °C in the absence of oxygen and at atmospheric pressure to generate bio-oil, char, and gases (Kawamoto 2017).

Selective, high yield transformations of lignin into low molecular weight value-added chemicals *via* direct pyrolysis has been studied in great detail for many years (Li *et al*. 2015), but little progress has been made toward industrialization. The most important cause of this may be a lack of systematic theory to guide lignin depolymerization arising from the complexity of the lignin macromolecule (Kawamoto 2017). To address these challenges, fast pyrolysis of lignin model compounds is used to simplify the pyrolysis processes; this approach provides an effective way to study the mechanism of lignin pyrolysis (Klein 1983; Britt *et al*. 2000; Chen *et al*. 2015; Watanabe *et al*. 2015; Kawamoto and Saka 2017). Especially, the β-aryl-ether linkages that are highlighted in blue color in Fig. S1a are ubiquitous and the most abundant lignin linkage, so the investigation of β–O–4 bond cleavage has received the greatest attention. Klein (1983) proposed a six-centered retro-ene mechanism from kinetic analysis of the formation of styrene and phenol from phenethyl phenyl ether (PPE). Britt *et al*. (2000) studied the substituent effects of the C_β-phenyloxy groups on the cleavage reactivity and proposed several ionic and radical mechanisms for explaining pyrolytic cleavage of the β-ether bond. Watanabe *et al*. (2015) studied pyrolytic reactivities of deuterated β-ether-type lignin model dimers and found that hydrogen abstractions from C_α and hydroxyl groups played direct roles in pyrolytic β-ether cleavage reactions. Kawamoto *et al*. (2007, 2008, 2017) studied the role of substituent groups in char formation from lignin-related compounds. They observed the homolysis of the O–CH_3 bond to form methyl and pyrocatechol radicals and radical-induced rearrangement of aromatic OCH_3 into aromatic CH_3 structures were two important reactions, and put forward the existence of C_α–OH caused by the formation of condensed lignin or oligomer. The above previous studies together confirmed that substituent groups on the side-chain and aromatic ring have a significant effect on the pyrolytic behavior of lignin models and enrich the understanding of the lignin pyrolysis mechanism.

Following the progression of the experimental research of lignin pyrolysis mechanisms, it was found that highly reactive lignin side-chain (benzylic) carbocations (Fig. S1c) could attack electron-rich lignin aromatic rings, resulting in the secondary condensation of monomers (Wang *et al*. 2016). Based on this above theoretical research result, some scholars sought to finding how to inhibit the formation of benzylic carbocations. Hence, some promising modification methods of C_α–OH were first developed for facilitating the subsequent cleavage of lignin chemical bonds, such as the

reduction of C_α–OH to C_α–H, etherification of C_α–OH to C_α–OCH_3 (Zhu *et al*. 2016), acetylation of C_α, γ–OH to C_α, γ–$OOCCH_3$ (Lohr *et al*. 2015), and chemoselective oxidation of C_αH−OH to C_α=O (Jiang *et al*. 2017; Zhang *et al*. 2017). Those methods were confirmed to increase the cleavage reactivity of the β–O–4 bond *via* effectively decreasing the barrier of chemical bonds. Particularly, oxidation of the benzylic alcohol group (Fig. S1b) received more attention due to its low cost and technological simplicity (Jiang *et al*. 2017). However, there have been numerous reports on substituent groups in aromatic rings for the cleavage of β–O–4 linkages in lignin model compounds, but relatively few reports of how those substituent groups affect pre-oxidized lignin model compounds that also contain a large number of oxygen functional groups, especially phenolic hydroxyl and methoxyl groups, which should also play a key role in β–O–4 cleavage reactions and products distribution.

Hence, three dimers (Fig. 1) were synthesized to represent β-ether-type lignin fragments. These dimer models contained both the typical β-aryl-ether linkages and primary aromatic units and contained different oxygen functional groups. Pyrolysis characteristics of three β-ether-type polymers were investigated by a simultaneous thermal analysis instrument (STA), *in-situ* Fourier transform infrared spectroscopy (*in-situ* FTIR), and pyrolysis-gas chromatography/mass spectrometry (Py-GC/MS), and the specific product distributions and migration patterns of volatile functional groups with temperature were monitored in real time. The relationships between pyrolysis conditions and product characteristics were proposed explaining the pyrolytic reactivity of pre-oxidized lignin.

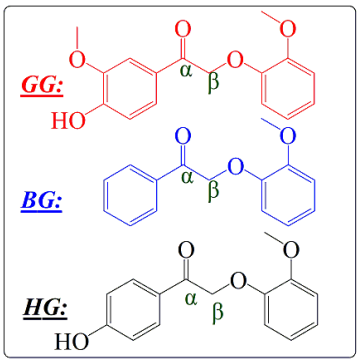

Fig. 1. The molecular structures of three C_α=O type model compounds. GG: 1-(4-hydroxy-3-methoxy-phenyl)-2-(2-methoxy-phenoxy)-ethanone; BG: 2-(2-methoxy-phenoxy)-1-phenyl-ethanone; HG: 1-(4-hydroxy-phenyl)-2-(2-methoxy-phenoxy)-ethanone

EXPERIMENTAL

Materials

Organic solvents, including methanol, ethyl acetate, petroleum ether, dichloro-methane, and so on, were purchased from Aladdin Chemistry Co., Ltd. (Shanghai, China). The reactants, such as guaiacol, 2-bromo-1-phenyl-ethanone, 2-bromo-1-(4-hydroxyl-phenyl)-ethanone, 2-bromo-1-(4-hydroxyl-3-methoxy-phenyl)-ethanone, and so on, were purchased from Alfa Aesar Co. Inc. (Wuhan, China). All chemicals were used without further purification. The lignin model compounds (Fig. 1) were prepared according to the published methods (Zhao *et al*. 2018) and detailed data are shown in supplementary material.

Experimental Methods

The thermal stability of three β–O–4-type model compounds was analyzed using a simultaneous thermal analysis instrument (STA449 F3; NETZSCH, Germany). Approximately 10 mg of sample was used for each test. The temperature was raised from room temperature to 650 °C under heating rates of 20 °C /min. The measurements were taken using high purity N_2 with a protective gas flow rate of 25 mL/min and a purge gas flow rate of 50 mL/min.

The *in-situ* diffuse reflectance infrared pyrolysis system used Fourier transform infrared spectroscopy (*in-situ* FTIR) (Nicolet IS50; Thermo Fisher Scientific Company, Waltham, MA, USA) and an *in-situ* pool with a deuterated sulfuric acid detector. To ensure full beam transmittance and good heat resistance, CaF_2 with protective water-cooling was employed as the window. The real time temperature of the *in-situ* pool was adjusted using a temperature controller with a PID (proportion, integration, and differentiation) thermo-coupling controller, and the accuracy of the temperature control was ± 1 °C. Specific operation parameters were as follows: nitrogen with purity of 99.999% was used to purge the system at a rate of 1 L/min for 15 min to maintain an inert atmosphere, after which the intake and outlet valves were closed to ensure that the pyrolysis process was carried out under sealed conditions. The temperature was increased from room temperature to 670 °C at a rate of 40 °C /min and was held at 670 °C for 10 min. The spectral scanning range was 650 to 4000 cm^{-1}, the resolution was 4 cm^{-1}, and the sampling interval was 1.93 s. A N_2 atmosphere at 100 °C was selected as the spectral background. The absence of interference from the purge gas on FTIR spectra of the pyrolysis vapors was ensured by a flat baseline corresponding to the beginning period.

Fast pyrolysis experiments of three dimers were conducted using a pyrolyzer (Tandem u-Reactor Rx-3050TR, Frontier Laboratories Ltd., Koriyama, Japan) having a direct connection to a gas chromatograph coupled with a mass spectrometer (GC/MS) (Agilent 7890B; Agilent Technologies, USA). In each experiment, 0.5 mg dimer was placed in a quartz filler tube. The pyrolysis temperature was set from room temperature to different terminal temperatures of 400, 450, 500, 550, and 600 °C and a fixed residence time of 20 s. The pyrolysis volatiles were analyzed online by GC/MS. The transfer line and injector temperature were kept at 300 °C. The chromatographic separation was performed using a TR-5MS capillary column (30 m × 0.25 mm i.d., 0.25 μm film thickness). Helium (99.999%) was used as the carrier gas with a constant flow rate of 1 mL/min and a 1:80 split ratio. The oven temperature was programmed from 40 °C (3 min) to 380 °C (3 min) at the heating rate of 4 °C /min. The temperature of the GC/MS interface was held at 300 °C, and the mass spectrometer was operated in EI mode at 70 eV. The mass spectra were obtained from m/z 20 to 400 with the scan rate of 500 amu^{-1}. Identification of chromatographic peaks was achieved according to the retention time and by matching the mass spectrum with the standards in the spectral library. Each run was replicated three times, and then the average data was used to calculate the relative area and relative yields of products.

RESULTS AND DISCUSSION

Thermal Stability Analysis

The thermogravimetry (TG) and differential thermogravimetry (DTG) curves for the three β–O–4-type lignin model compounds under N_2 atmosphere at a heating rate of 20

°C /min are shown in Fig. 2. At an early stage, ranging from room temperature to 150 °C, a low weight loss was mainly attributed to moisture and organic solvent that was retained during synthesis. In the fast degradation stage, ranging from 150 to 400 °C, most of the models were converted into volatiles. As determined from the DTG curves (Fig. 2b), the main weight loss peaks of BG, GG, and HG appeared at 245 °C, 308 °C, and 320 °C, respectively. For HG and GG, the main depolymerization stage was 200 to 400 °C and 200 to 350 °C, respectively. The difference between HG and GG was substituent groups (–OCH_3) on the aromatic ring, suggesting that the –OCH_3 on the aromatic rings enhanced the activity of the intermolecular linkages and decreased its thermal stability. Similar results were reported previously (Li *et al*. 2016; Zhao *et al*. 2018). In the slow degradation stage, the char yield of HG was approximately 10%, which was higher than the char yields of GG and BG (approximately 2%). In summary, substituent groups of aromatic rings had an effect on not only thermal stability of models, but also coke formation.

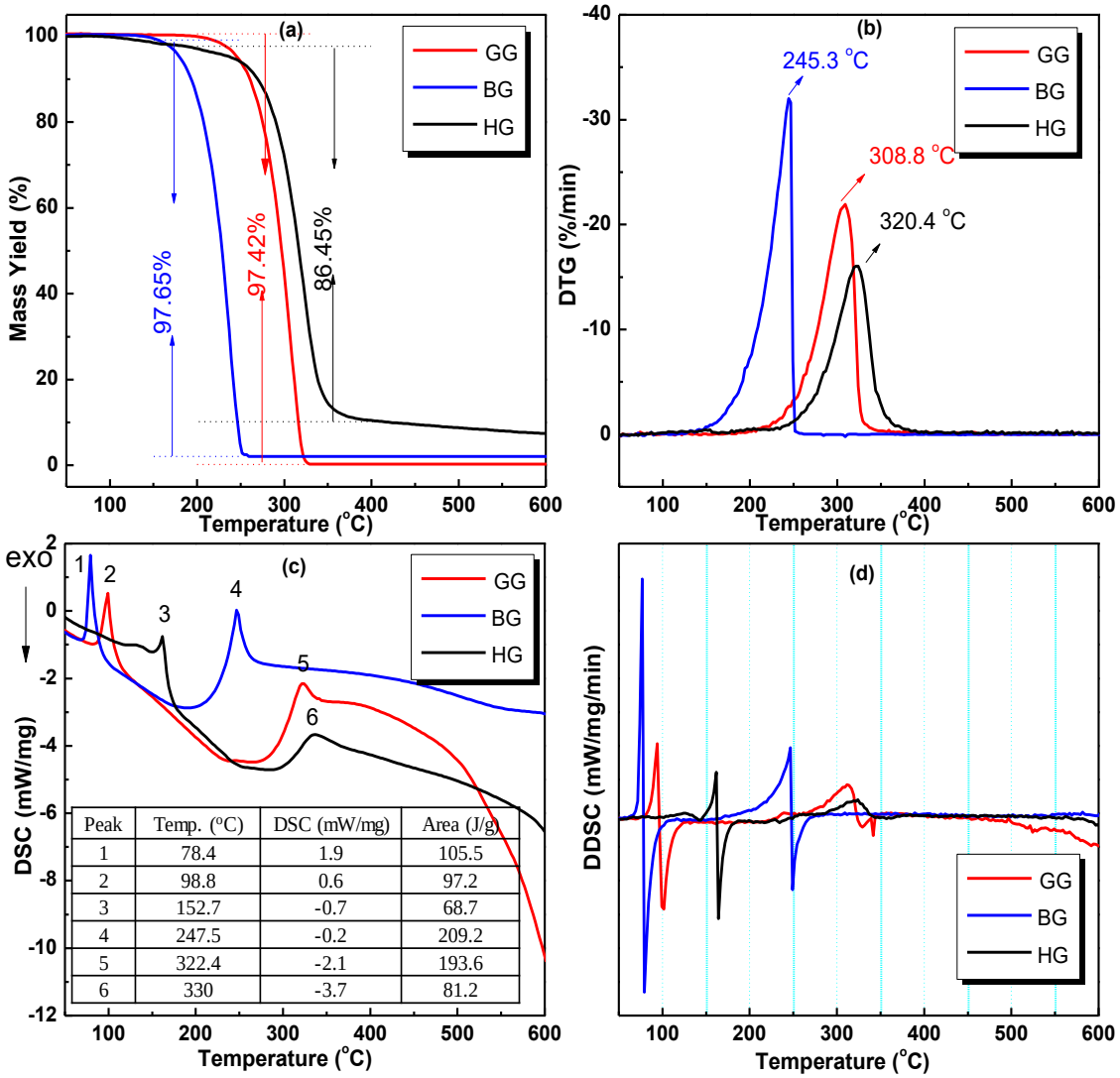

Peak	Temp. (°C)	DSC (mW/mg)	Area (J/g)
1	78.4	1.9	105.5
2	98.8	0.6	97.2
3	152.7	-0.7	68.7
4	247.5	-0.2	209.2
5	322.4	-2.1	193.6
6	330	-3.7	81.2

Fig. 2. TG, DTG, differential scanning calorimetry (DSC) and dynamic differential scanning calorimetry (DDSC) curves of three dimers

Main Functional Groups of Volatiles

The FTIR spectra of pyrolysis volatiles at 500 °C and the assignments of spectral peaks are displayed in Fig. 3. Major functional group vibrations (Li *et al*. 2016; Jiang *et al*. 2017) were classified into the following nine categories. The real-time monitoring results of volatiles are visible in Fig. S2, showing the evolution of major functional groups occurred in the range of 200 to 400 °C. It was in line with the mass loss result of TG, where the maximum weight loss rate temperature was 245 °C (BG), 308 °C (GG), and 320 °C (HG).

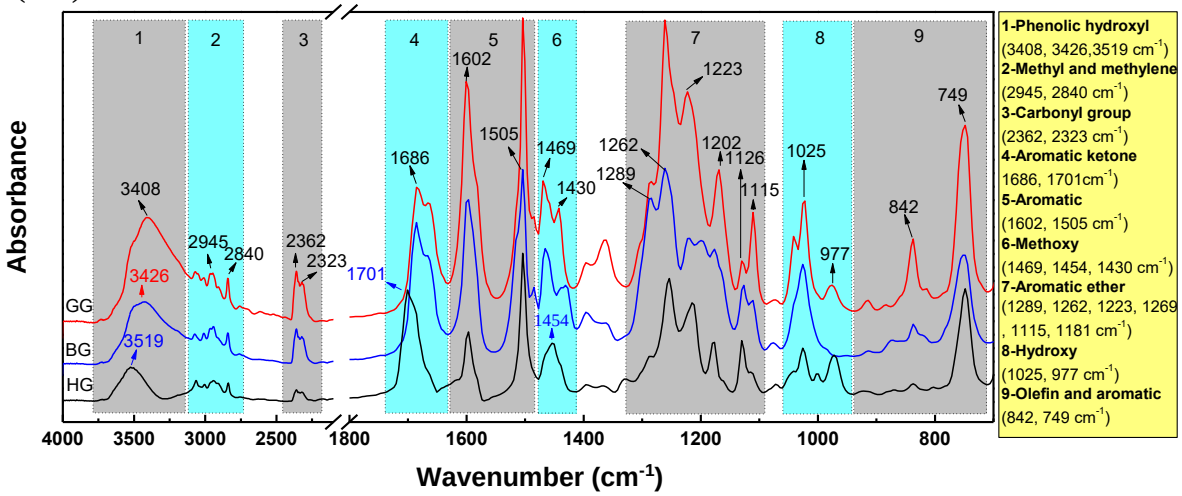

Fig. 3. FTIR spectra of three dimers at 500 °C

Variation in absorption intensity of BG pyrolysis was monitored in real time and analyzed semi-quantitatively using the peak height (represented by blue line in Fig. S2). At the beginning, an increase involving alcoholic hydroxyl and methyl groups was found in Fig. S3 (a) and (d), it was speculated that small molecular alcohols (methyl alcohol) were released as a residual solvent. The absorption intensity of the carbonyl group grew rapidly between 250 °C and 400 °C and began to level off at higher temperatures (> 400 °C). This indicated that a large amount of volatile products with carbonyl groups were generated within the range 250 to 400 °C, and the volatile products had relatively high stability during the whole pyrolysis process. Intramolecular hydrogen bond vibration of the phenolic hydroxyl functional groups at 3426 cm^{-1}, C=C stretching vibration of aromatic groups at 1602 cm^{-1}, and C=O stretching vibration of the aromatic ketone at 1686 cm^{-1} were first detected at 250 °C, after which their intensity increased with pyrolysis temperature increase to 300 °C. This was because the monomeric aromatics with phenolic –OH and $–COCH_3$ groups were formed *via* the cleavage of the C_β–O bond. With further temperature increases to 320 °C, absorption intensity declined. The $–CH_3$ group at 2362 cm^{-1} and $–CH_2–$ at 2323 cm^{-1} were weak at low temperature, suggesting that the reaction involved the removal of methyl and methylene groups in aliphatic substructures was difficult. As to GG, variation in absorption intensity of specific functional groups is shown in Fig. S2 (represented by the red line). Intramolecular hydrogen bond vibration of the phenolic hydroxyl functional groups was detected from 230 °C that rapidly increased in intensity with temperature increase to 300 °C, and then slowly increased. The peak corresponding to the emission of C=O, which appeared at approximately 300 °C, also increased in intensity with temperature. As compared to other models, its absorption intensity was higher, suggesting the higher yield. The peaks of methyl and methylene showed no changes before 200 °C and then they

rapidly increased between 250 and 300 °C. Liu *et al*. (2008) reported that CH_4 was mainly attributed to the demethylation of methoxy (–OCH3), methyl (–CH_3), and methylene (–CH_2) groups *via* homolytic cleavage of the O–CH_3 bond. It was suggested that the demethylation occurred in the range 200 to 300 °C. In addition, the concentrations of methoxy, aromatic ketone, aromatic, aromatic ethers, and hydroxyl all increased between 250 and 300 °C. This indicated that the cleavage of C_α–C_β and C_β–O bonds mainly occurred between 250 and 300 °C. This agreed with the maximum weight loss temperature range of GG. The absorbance intensity variation of HG with temperature is shown in Fig. S2, represented by black line. Almost all the change trend of absorption peaks was similar with GG and BH. However, an obvious difference was that the absorption intensity was lower, especially for aromatic, carbon dioxide, carbon monoxide, and methyl and methylene groups. Such a finding indicated that the HG was more difficult to decompose compared with the GG and BG and produced less aromatics.

During the model compounds' pyrolysis, strong vibrations of aromatic rings at 1602 and 1505 cm^{-1} were evidence that aromatic compounds were the major pyrolysis products. The aromatic absorbance values of BG were nearly doubled compared to that of GG at 300 to 550 °C, indicating that BG was converted into a higher concentration of aromatic monomeric products during pyrolysis. Combining with the TG data, where most of models were converted into volatiles, it can be speculated that adding the –OCH_3 group to the ring was beneficial for promoting the formation of high molecular weight oligomer, and it led to the lower yield of aromatics. With increasing temperature, the peak value of aromatics reached maximum at 300 °C (GG), 320 °C (BG), and 265 °C (HG). Then, there was a general decreasing tendency for the concentration within a shorter time period. The process was attributed to the secondary reaction of major monomeric aromatics. As the temperature continued to increase, the intensity gradually increased due to the pyrolysis of new oligomers at higher temperatures. The peak intensity corresponding to the aromatic ketone at 1686 and 1701 cm^{-1} and aromatic structures at 1602 and 1505 cm^{-1} was detected earlier than small molecular gas components (CO and CO_2). Such a result indicated that cleavage of intermolecular linkages dominated at low temperatures, followed by secondary reaction (Jiang *et al*. 2017). Additionally, aromatic ketones and aromatics, as the primary pyrolysis products, provided various gas and low-molecular-weight compounds. Just like the HG-type model compound, the peak corresponding to aromatic ketone at around 1701 cm^{-1} rapidly increased in intensity between 200 and 275 °C, slightly decreased after 275 °C, and at last leveled off. The absorbance values of the phenolic hydroxyl always increased in intensity between 200 and 350 °C and then gradually increased after 400 °C. This suggested that phenolic hydroxyl groups were highly stable. In contrast, the intensity of the absorption involving to aromatic ketone, aromatics, methyl, and methylene grew rapidly between 250 °C and 300 °C and later declined before at last leveling off. This suggested that aromatic ketone, aromatics, and methyl and methylene groups could be transformed into downstream products by secondary reactions. In addition, the CO_2 emission peak for the three samples was similar, beginning at approximately 300 °C and then intensifying with increasing temperature. This indicated that the decarboxylation reaction began at 300 °C. However, the intensity of the CO_2 absorption peak from GG was higher than HG, suggesting that the methoxy group improved the level of decarboxylation.

The Evolution of Pyrolytic Products During Fast Pyrolysis

Representative pyrograms at 500 °C are shown in Fig. 4. Approximately 10 kinds of phenolic products or aromatic hydrocarbons with a high degree of matching (at least

98%) are listed in Tables 1 through 3. According to the aromatic substituent groups and the products origin, the detected compounds were divided into three categories (Fig. S4): (1) Ring A products (RAP), *i.e.*, benzaldehyde, acetophenone, vanillin, acetovanillone, 4-hydroxy-benzaldehyde, and 4-hydroxy-acetophenone; (2) Ring B products (RBP), *i.e.*, guaiacol and 2-methoxy-benzaldehyde; (3) RAP and RBP derivatives (RD), including phenol, 2-methylphenol, 4-methylphenol, *etc*. Based on Py-GC/MS, the evolution of content for RAP, RBP, RD is shown in Fig. 5(a), Fig. 5(b), and Fig. 6, respectively.

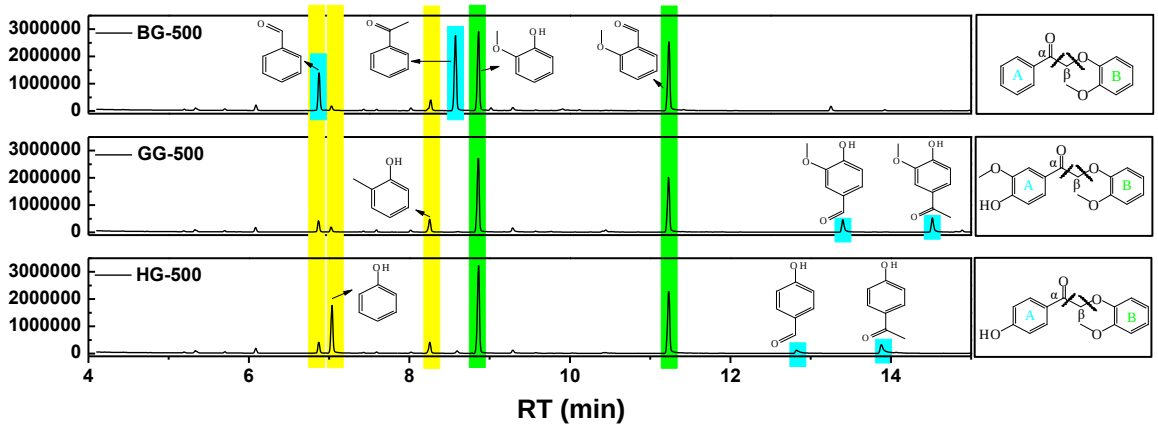

Fig. 4. GC–MS chromatogram of three models obtained at 500 °C

As shown in Table 1, the main pyrolysis products of BH were benzaldehyde, phenol, 2-methylphenol, acetophenone, guaiacol, and 2-methoxy-benzaldehyde. Among these, RBP, obtained *via* the cleavage of C_β–O bonds, predominated at low temperatures (400 °C), and the total relative content was 57.5%.

Table 1. Distribution of Main Pyrolytic Products from the BG Under Different Temperatures (Amount in Relative area (%))

NO.	Compounds	RT (min)	Pyrolysis Temperature (°C)				
			400	450	500	550	600
5	Benzaldehyde	6.87	5.0	7.4	9.7	10.0	10.3
6	Phenol	7.03	0.4	0.5	1.2	3.8	5.2
11	2-Methylphenol	8.27	0.0	0.5	3.3	8.0	8.3
12	Acetophenone	8.58	14.6	16.9	21.5	27.1	32.0
13	Guaiacol	8.86	30.0	27.9	22.3	9.6	6.0
24	2-Methoxy-benzaldehyde	11.23	27.5	24.0	21.2	13.2	8.9
Total peak area percentage			77.5	77.2	79.2	71.5	70.6

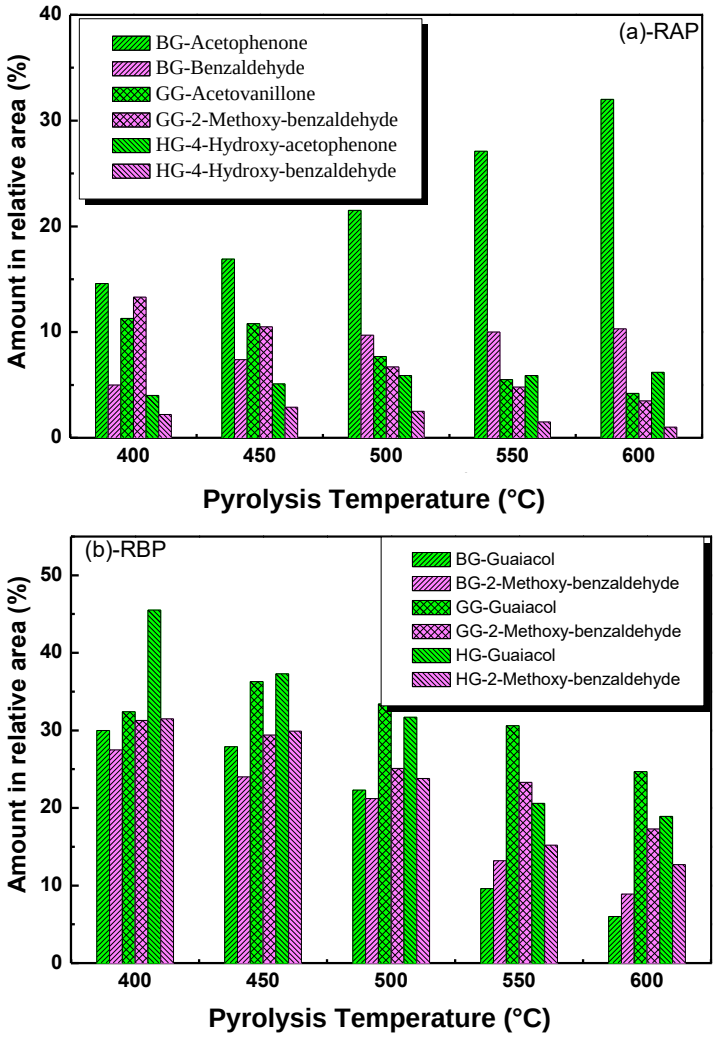

Fig. 5. The evolution of content for several selected components from ring A and B based on the results of Py-GCMS

The most representative compounds were guaiacol and 2-methoxy-benzaldehyde, with peak areas (%) of 30.0% and 27.5%, respectively. Additionally, benzaldehyde and 2-methoxy-benzaldehyde, as RAP, was the product of ring A *via* the cleavage of C_α–C_β bond, and had the second highest peak areas (%) of approximately 20% at 400 °C. Based on the previous "Thermal Stability Analysis" and "Main Functional Groups of Volatiles" experimental data, and the result of Py-GC/MS where no models samples were detected, it can be verified that BG was decomposed completely at 400 °C. In other words, RAP and RBP were generally originated from the direct splitting of the ring A and B unit *via* the cleavage of C_α–C_β and C_β–O bonds of the BG structure at 400 °C. In addition, RD generally originated from the secondary cracking reactions, and its concentrations were lowest at 400 °C, as compared to RAP and RBP.

As shown in Fig. 5, phenol was detected as a representative RD at 400 °C at only 0.4%. It was likely formed *via* the transformation of RBP. As temperatures increased from 400 °C to 600 °C, RBP decreased rapidly, while RAP and RD increased. For example, guaiacol and 2-methoxy-benzaldehyde decreased from 30.0% and 27.5% to 6.0% and 8.9%, respectively. Meanwhile, benzaldehyde and acetophenone increased from 5.0% and 14.6% to 10.3% and 32.0 %, respectively.

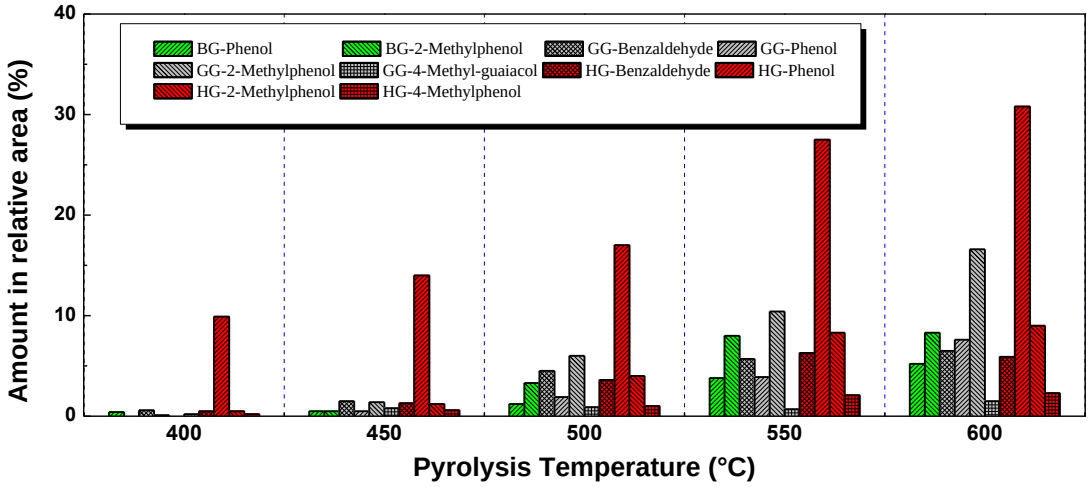

Fig. 6. The evolution of content for several secondary reaction components based on the results of Py-GCMS

As temperatures increase to 600 °C, RAP became the main compounds, and the total peak area could come up to 42.3%. Particularly, acetophenone, as a representative RAP, had a concentration of 32.0%. In addition, 2-methylphenol, as a representative RD like phenol, was first detected at 450 °C. Its yield increased to 8.3% at 600 °C. This suggested that more products occurred in secondary reactions, and the intensity was increasingly stronger with pyrolysis temperature increase.

Table 2 shows that the main pyrolytic products from the GG were vanillin (13.3%), acetovanillone (11.3%), guaiacol (32.4%), and 2-methoxy-benzaldehyde (31.3%) at 400 °C. It was clear that four compounds were formed *via* the cleavage of C_{α}–C_{β} and C_{β}–O bonds and not secondary reactions. The result indicated that four pyrolysis products sustained a fine stability at low temperature. When the temperature increased to 600 °C, the content of 2-methoxy-benzaldehyde, vanillin, and acetovanillone decreased to 17.3%, 3.5%, and 4.2%, respectively.

Meanwhile, RD (benzaldehyde, phenol, 2-methylphenol, and 4-methyl-guaiacol) increased, particularly 2-methylphenol, and it increased to 16.6%. It had been reported that 2-methylphenol was converted by guaiacol, which occurred after the rearrangement of aryl–OCH_3 into aryl–CH_3 structure. Additionally, guaiacol had a higher proportion compared to that from BG. Based on the above result, it was speculated that vanillin and acetovanillone were unstable during the pyrolysis process, and both might play an important role on the formation of guaiacol, 2-methylphenol, and 4-methyl-guaiacol *via* side-chain-conversion. Hence, data on thermal reactivity and secondary pyrolysis pathways of vanillin and acetovanillone was also studied *via in-situ* FTIR within a tube furnace reactor system (Jiang *et al*. 2018). The result indicated that vanillin had higher reactivity than acetovanillone. The removal of the –CHO group in vanillin was observed at 400 °C. Overall, guaiacol could have been obtained *via* the cleavage of C_{β}–O bonds and also through removal of –CHO from vanillin.

Table 2. Distribution of Main Pyrolytic Products from the GG Under Different Temperatures (Amount in Relative Area (%))

No.	Compounds	RT (min)	Pyrolysis Temperature (°C)				
			400	450	500	550	600
5	Benzaldehyde	6.87	0.6	1.5	4.5	5.7	6.5
6	Phenol	7.04	0.1	0.5	1.9	3.9	7.6
11	2-Methylphenol	8.25	0.0	1.4	6.0	10.4	16.6
14	Guaiacol	8.87	32.4	36.3	33.4	30.6	24.7
20	4-Methyl-guaiacol	10.45	0.2	0.8	0.9	0.7	1.5
23	2-Methoxy-benzaldehyde	11.24	31.3	29.4	25.1	23.3	17.3
25	Vanillin	13.41	13.3	10.5	6.7	4.8	3.5
28	Acetovanillone	14.52	11.3	10.8	7.7	5.5	4.2
Total peak area percentage			89.0	90.5	85.4	84.1	80.5

Table 3. Distribution of Main Pyrolytic Products from the HG Under Different Temperatures (Amount in Relative Area (%))

No.	Compounds	RT (min)	Pyrolysis Temperature (°C)				
			400	450	500	550	600
5	Benzaldehyde	6.87	0.5	1.3	3.6	6.3	5.9
6	Phenol	7.04	9.9	14.0	17.0	27.5	30.8
11	2-Methylphenol	8.26	0.5	1.2	4.0	8.3	9.0
12	4-Methylphenol	8.59	0.2	0.6	1.0	2.1	2.3
13	Guaiacol	8.86	45.5	37.3	31.7	20.6	18.9
24	2-Methoxy-benzaldehyde	11.23	31.5	29.9	23.8	15.2	12.7
30	4-Hydroxy-benzaldehyde	12.85	2.2	2.9	2.5	1.5	1.0
33	4-Hydroxy-acetophenone	13.89	4.0	5.1	5.9	5.9	6.2
Total peak area percentage			94.4	92.1	89.5	87.3	86.8

As to HG, the main pyrolysis products (Table 3) included phenol, guaiacol, and 2-methoxy-benzaldehyde at 400 °C. Similar to the BG and GG type model compound, 2-methoxy-benzaldehyde and guaiacol were also two important products from Ring B *via* the cleavage of C_β–O and C_α–C_β bonds, whose yield were 45.5% and 31.5% at 400 °C, respectively. As the typical RAP-type pyrolysis products, 4-hydroxy-benzaldehyde and 4-hydroxy-acetophenone were only 2.2% and 4.0%, respectively, which indicated that RAP might play an important role on polymerization and side-chain-conversion during the pyrolysis process. Meanwhile, phenol (9.9%) was detected at 400 °C, and it was different from the pyrolysis product distribution for BG and HG. Based on the structure characteristics of the product, it was deduced that phenol could be obtained *via* many kinds of secondary reaction pathways. As described in the previous section, guaiacol could be an important precursor, and it was in the habit of removal of $–OCH_3$ for formation of phenol at higher temperature. In addition, the removal of the –CHO group from 4-hydroxy-benzaldehyde could be another reason. When the temperature increased to 600 °C, the percentage of 4-hydroxy-benzaldehyde was only 1.0%. Meanwhile, the yield of phenol increased to 30.8%, and it was higher than that of BG (0.4%) and GG (0.1%). This meant that most of the removal of -CHO from 4-hydroxy-benzaldehyde occurred at 600 °C.

Hence, the –CHO removal of 4-hydroxy-benzaldehyde was considered to be the dominating pathway for phenol formation.

In summary, oxidization of benzylic alcohol (C_α–OH) to benzylic ketone (C_α=O) not only facilitated the cleavage of C_α–O and C_α–C_β bonds (Jiang *et al*. 2018), but it also simplified depolymerization pathways, resulting in better selectivity of phenolic monomers and a predictable product distribution. Generally, the pyrolysis process included primary and secondary reactions (Scholze and Meier 2001). As shown in Figs. 4 and 5, monomeric compounds RAP and RBP are regarded as primary products derived directly from pyrolysis and are also regarded as the intermediates that occur in the secondary reactions for the formation of RD due to substituted groups and aromatic nucleus. Affected by the substituents, primary products showed different reaction activity. For instance, RAP (benzaldehyde and acetophenone) were the typical products of ring A *via* the direct cleavage of the C_β–O and C_α–C_β bond. The high stability at 400 to 600 °C and the peak area ratio of benzaldehyde and acetophenone could reflect the cleavage ratio of C_α–C_β and C_β–O bonds. During the pyrolysis process, the cleavage ratio of the C_β–O was 68 to 76%, which indicated that the cleavage of the C_β–O bond was primary compared with that of C_α–C_β. This is mainly because the dissociation energy of C_β–O was lower than that of C_α–C_β; therefore, the homolytic cleavage of C_β–O bonds dominated over the C_α–C_β homolytic reactions in the pyrolysis process (Britt *et al*. 2000). Meanwhile, guaiacol and 2-methoxy-benzaldehyde, as RBP, were also important products from primary reaction. Guaiacol mainly was formed through combination of the guaiacyl radical with free H radicals after C_β–O homolytic reaction (Li *et al*. 2016; Zhu *et al*. 2016). During the C_α–C_β homolytic reactions (Jiang *et al*. 2017), 2-methoxy-benzaldehyde was obtained through a series of reactions after breaking the C_α–C_β bond, and the optimized geometries of reactants, intermediates, transition states, and products in pyrolysis processes had been reported in previous literature (Yanez *et al*. 2018). Based on the product's structure, guaiacol and 2-methoxy-benzaldehyde were considered as two important intermediates that can occur in the secondary reactions. Phenol and 2-methylphenol were the typical downstream products and were converted *via* secondary reactions of RBP. A schematic diagram of the proposed mechanism of guaiacol and 2-methoxy-benzaldehyde is shown in Fig. S5. At low pyrolysis temperature, guaiacol can convert into phenol through the release of $–OCH_3$. At higher pyrolysis temperatures guaiacol was converted into 2-methylphenol *via* radical-induced rearrangement of the aryl–OCH_3 group into the aryl–CH_3 group. The aryl–OCH_3 group into the aryl–CH_3 group was more competitive than the removal of $–OCH_3$. For GG and HG model compounds, the secondary reaction of RBP (guaiacol and 2-methoxy-benzaldehyde) was in agreement with BG. However, affected by the substituents (phenolic hydroxyl and methoxy), RAP showed higher reaction activity.

CONCLUSIONS

1. Substituent groups of aromatic rings had an effect on thermal stability of model compounds, emission of volatiles, and the evolution of pyrolytic products. Particularly, the $–OCH_3$ on the aromatic rings played an important role for enhancing the activity of the intermolecular linkages and decreasing its thermal stability.
2. Pyrolysis of pre-oxidized β-ether-type lignin models mainly included two pathways: (a) cleavage of C_α–C_β and C_β–O bonds; and (b) secondary pyrolysis of monomeric

aromatics. Oxidation of the C_α–OH group into C_α=O could effectively curb the formation of new dimers, resulting in better selectivity of phenolic monomers and a predictable product distribution.

3. Volatile products mainly included large amounts of guaiacol and 2-methoxy-benzaldehyde and their derived aromatics. Among these, guaiacol and 2-methoxy-benzaldehyde were two important intermediates, and secondary reactions mainly occurred *via* the rearrangement and removal of aryl–OCH_3.

ACKNOWLEDGMENTS

This work was supported by National Natural Science Foundation of China (Nos. 31901266 and 31770626) and the Foundation (No. ZZ20190101) of State Key Laboratory of Bio-based Material and Green Papermaking, Qilu University of Technology, Shandong Academy of Sciences.

REFERENCES CITED

Boerjan, W., Ralph, J., and Baucher, M. (2003). "Lignin biosynthesis," *Annual Review of Plant Biology* 54(1), 519-546. DOI: 10.1146/annurev.arplant.54.031902.134938

Britt, P. F., Buchanan, A. C., Cooney, M. J., and Martineau, D. R. (2000). "Flash vacuum pyrolysis of methoxy-substituted lignin model compounds," *Journal of Organic Chemistry* 65(5), 1376-1389. DOI: 10.1021/jo991479k

Chen, L., Ye, X., Luo, F., Shao, J., Lu, Q., Fang, Y., Wang, X., and Chen, H. (2015). "Pyrolysis mechanism of β-O-4 type lignin model dimer," *Journal of Analytical and Applied Pyrolysis* 115, 103-111. DOI: 10.1016/j.jaap.2015.07.009

Chen, W. H., and Kuo, P. C. (2011). "Torrefaction and co-torrefaction characterization of hemicellulose, cellulose and lignin as well as torrefaction of some basic constituents in biomass," *Energy* 36(2), 803-811. DOI: 10.1016/j.energy.2010.12.036

Crestini, C., Lange, H., Sette, M., and Argyropoulos, D. S. (2017). "On the structure of softwood kraft lignin," *Green Chemistry* 19(17), 4104-4121. DOI: 10.1039/C7GC01812F

Farag, S., and Chaouki, J. (2015). "Economics evaluation for on-site pyrolysis of kraft lignin to value-added chemicals," *Bioresource Technology* 175, 254-261. DOI: 10.1016/j.biortech.2014.10.096

Han, T., Sophonrat, N., Evangelopoulos, P., Persson, H., Yang, W. H., and Jonsson, P. (2018). "Evolution of sulfur during fast pyrolysis of sulfonated Kraft lignin," *Journal of Analytical and Applied Pyrolysis* 133, 162-168. DOI: 10.1016/j.jaap.2018.04.006

Jiang, W. K., Wu, S. B., Lucia, L. A., and Chu, J. Y. (2017). "A comparison of the pyrolysis behavior of selected β-O-4 type lignin model compounds," *Journal of Analytical and Applied Pyrolysis* 125, 185-192. DOI: 10.1016/j.jaap.2017.04.003

Jiang, W. K., Chu, J. Y.,Wu, S. B., and Lucia, L. A. (2018a). "Modeling pyrolytic behavior of pre-oxidized lignin using four representative β-ether-type lignin-like model polymers," *Fuel Processing Technology* 176, 221-229. DOI: 10.1016/j.fuproc.2018.03.041

Jiang, W. K., Chu, J. Y., Wu, S. B., and Lucia, L. A. (2018b). "Modeling the pyrolytic behavior of lignin through two representative monomers: Vanillin and acetovanillone," *Journal of Analytical and Applied Pyrolysis* 130, 241–248. DOI: 10.1016/j.jaap.2018.01.001

Kawamoto, H. (2017). "Lignin pyrolysis reactions," *Journal of Wood Science* 63(2), 117-132. DOI: 10.1007/s10086-016-1606-z

Kawamoto, H., Horigoshi, S., and Saka, S. (2007a). "Effects of side-chain hydroxyl groups on pyrolytic β-ether cleavage of phenolic lignin model dimer," *Journal of Wood Science* 53(3), 268-271. DOI: 10.1007/s10086-006-0839-7

Kawamoto, H., Horigoshi, S., and Saka, S. (2007b). "Pyrolysis reactions of various lignin model dimers," *Journal of Wood Science* 53(2), 168-174. DOI: 10.1007/s10086-006-0834-z

Kawamoto, H., Ryoritani, M., and Saka, S. (2008). "Different pyrolytic cleavage mechanisms of β-ether bond depending on the side-chain structure of lignin dimers," *Journal of Analytical and Applied Pyrolysis* 81(1), 88-94. DOI: 10.1016/j.jaap.2007.09.006

Kawamoto, H., and Saka, S. (2017). "Role of side-chain hydroxyl groups in pyrolytic reaction of phenolic β-ether type of lignin dimer," *Journal of Wood Chemistry & Technology* 27(2), 113-120. DOI: 10.1080/02773810701515119

Klein, M. T. (1983). "Model pathways in lignin thermolysis," *Industrial & Engineering Chemistry Research* 22(1), 35-45. DOI: 10.1021/i100009a007

Li, C. Z., Zhao, X. C., Wang, A. Q., Huber, G. W., and Zhang, T. (2015). "Catalytic transformation of lignin for the production of chemicals and fuels," *Chemical Reviews* 115(21), 11559-11624. DOI: 10.1021/acs.chemrev.5b00155

Li, P., Chen, L., Wang, X., Yang, H., Shao, J., and Chen, H. (2016). "Effects of oxygen-containing substituents on pyrolysis characteristics of β-O-4 type model compounds," *Journal of Analytical and Applied Pyrolysis* 120, 52-59. DOI: 10.1016/j.jaap.2016.04.009

Liu, Q., Wang, S., Zheng, Y., Luo, Z., and Cen, K. (2008). "Mechanism study of wood lignin pyrolysis by using TG–FTIR analysis," *Journal of Analytical and Applied Pyrolysis* 82(1), 170-177. DOI: 10.1016/j.jaap.2008.03.007

Lohr, T. L., Li, Z., and Marks, T. J. (2015). "Selective ether/ester C–O cleavage of an acetylated lignin model via tandem catalysis," *ACS Catalysis* 5(11), 7004-7007. DOI: 10.1021/acscatal.5b01972

No, S. Y. (2014). "Application of bio-oils from lignocellulosic biomass to transportation, heat and power generation-A review," *Renewable & Sustainable Energy Reviews* 40, 1108-1125. DOI: 10.1016/j.rser.2014.07.127

Ong, H. C., Chen, W. H., Farooq, A., Gan, Y. Y., Lee, K. T., and Ashokkumar, V. (2019). "Catalytic thermochemical conversion of biomass for biofuel production: A comprehensive review," *Renewable & Sustainable Energy Reviews* 113(109266), 1-16. DOI: 10.1016/j.rser.2019.109266

Ralph, J., Lapierre, C., and Boerjan, W. (2019). "Lignin structure and its engineering," *Current Opinion in Biotechnology* 56, 240-249. DOI: 10.1016/j.copbio.2019.02.019

Scholze, B., and Meier, D. J. (2001). "Characterization of the water-insoluble fraction from pyrolysis oil (pyrolytic lignin). Part I. PY–GC/MS, FTIR, and functional groups," *Journal of Analytical and Applied Pyrolysis* 60(1), 41-54. DOI: 10.1016/S0165-2370(00)00110-8

Wang, S., Ru, B., Dai, G., Shi, Z., Zhou, J., Luo, Z., Ni, M., and Cen, K. (2016). "Mechanism study on the pyrolysis of a synthetic β-O-4 dimer as lignin model compound," *Proceedings of the Combustion Institute* 36(2), 2225-2233. DOI: 10.1016/j.proci.2016.07.129

Watanabe, T., Kawamoto, H., and Saka, S. (2015). "Pyrolytic reactivities of deuterated β-ether-type lignin model dimers," *Journal of Analytical and Applied Pyrolysis* 112, 23-28. DOI: 10.1016/j.jaap.2015.02.028

Yanez, A. J., Natarajan, P., Li, W., Mabon, R., and Broadbelt, L. J. (2018). "Coupled structural and kinetic model of lignin fast pyrolysis," *Energy and Fuels* 32(2), 1822-1830. DOI: 10.1021/acs.energyfuels.7b03311

Zhang, C., Li, H., Lu, J., Zhang, X., MacArthur, K. E., Heggen, M., and Wang, F. (2017). "Promoting lignin depolymerization and restraining the condensation *via* an oxidation-hydrogenation strategy," *ACS Catalysis* 7(5), 3419-3429. DOI: 10.1021/acscatal.7b00148

Zhao, L., Shi, S., Liu, M., Zhu, G., Wang, M., Du, W., Gao, J., and Xu, J. (2018). "Covalent triazine frameworks catalytically oxidative cleavage of lignin models and organosolv lignin," *Green Chemistry* 20(6), 1270-1279. DOI: 10.1039/C8GC00268A

Zhu, G. D., Qiu, X. Q., Zhao, Y., Qian, Y., Pang, Y. X., and Ouyang, X. P. (2016). "Depolymerization of lignin by microwave-assisted methylation of benzylic alcohols," *Bioresource Technology* 218, 718-722. DOI: 10.1016/j.biortech.2016.07.021

Article submitted: April 28, 2020; Peer review completed: July 3, 2020; Revised version received and accepted: July 19, 2020; Published: July 23, 2020.
DOI: 10.15376/biores.15.3.6989-7008

SUPPLEMENTARY MATERIAL

Three types of model dimers were used in this study, and detailed data are shown below: (1) 1-(4-hydroxy-3-methoxy-phenyl)-2-(2-methoxy-phenoxy)-ethanone, referred to as GG; (2) 2-(2-methoxy-phenoxy)-1-phenyl-ethanone, referred to as BG; (3) 1-(4-hydroxy-phenyl)-2-(2-methoxy-phenoxy)-ethanone, referred to as HG. The chemical structures were confirmed by ^{1}H NMR and ^{13}C NMR.

GG: ^{1}H NMR (600 MHz, DMSO-d_6) δ 10.11 (s, 1H, aryl–OH), 7.59 to 6.80 (m, 7H), 5.43 (s, 2H), 3.84 to 3.78 (m, 6H); ^{13}C NMR (151 MHz, DMSO-d_6) δ 193.21 (C_α), 152.72, 149.45, 148.12, 148.04, 126.70, 123.36, 121.72, 121.01, 115.56, 114.10, 112.94, 111.65 (aryl C), 70.90 (C_β), 56.14, 56.03(–OCH_3).

BG: ^{1}H NMR (600 MHz, DMSO-d_6) δ 8.03 (m, 2H), 7.69 (m, 1H), 7.57 (m, 2H), 6.99 to 6.81 (m, 4H), 5.54 (s, 2H), 3.78 (s, 3H); ^{13}C NMR (151 MHz, DMSO-d_6) δ 194.6, 149.9, 147.6, 134.7, 128.8, 128.2, 122.6, 120.9, 115, 112.3, 72.2,56.

HG: ^{1}H-NMR (600 MHz, DMSO-d_6): 10.46 (s, 1H), 7.91 to approximately 6.79 (m, 8H), 5.40 (s, 2H), 3.78 (s, 3H); ^{13}C-NMR (151 MHz, DMSO-d_6): 193.16, 162.99, 149.50, 148.09, 130.96, 126.55, 121.75, 121.04, 115.84, 114.19, 113.03, 70.90, 56.08.

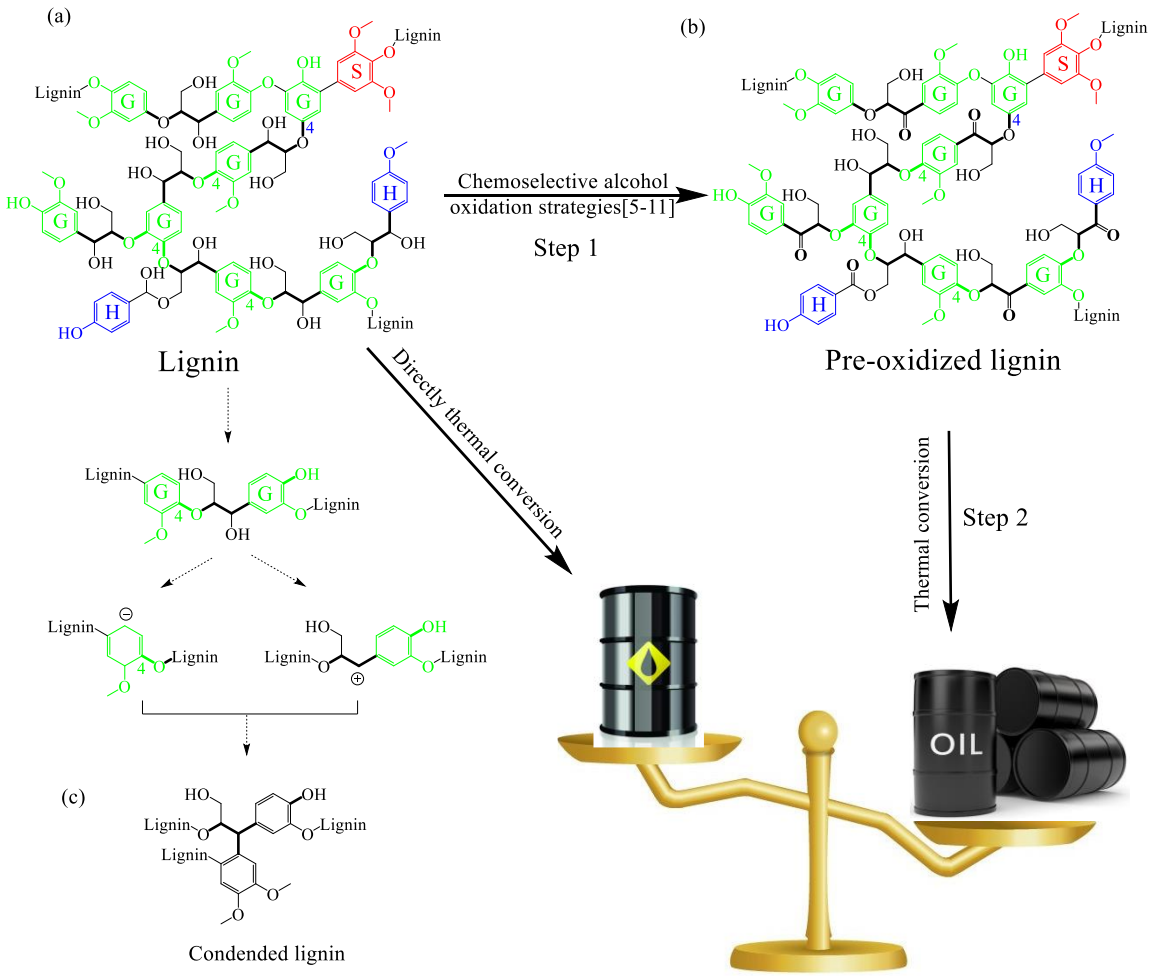

Fig. S1. Typical scheme of lignin oxidation depolymerization

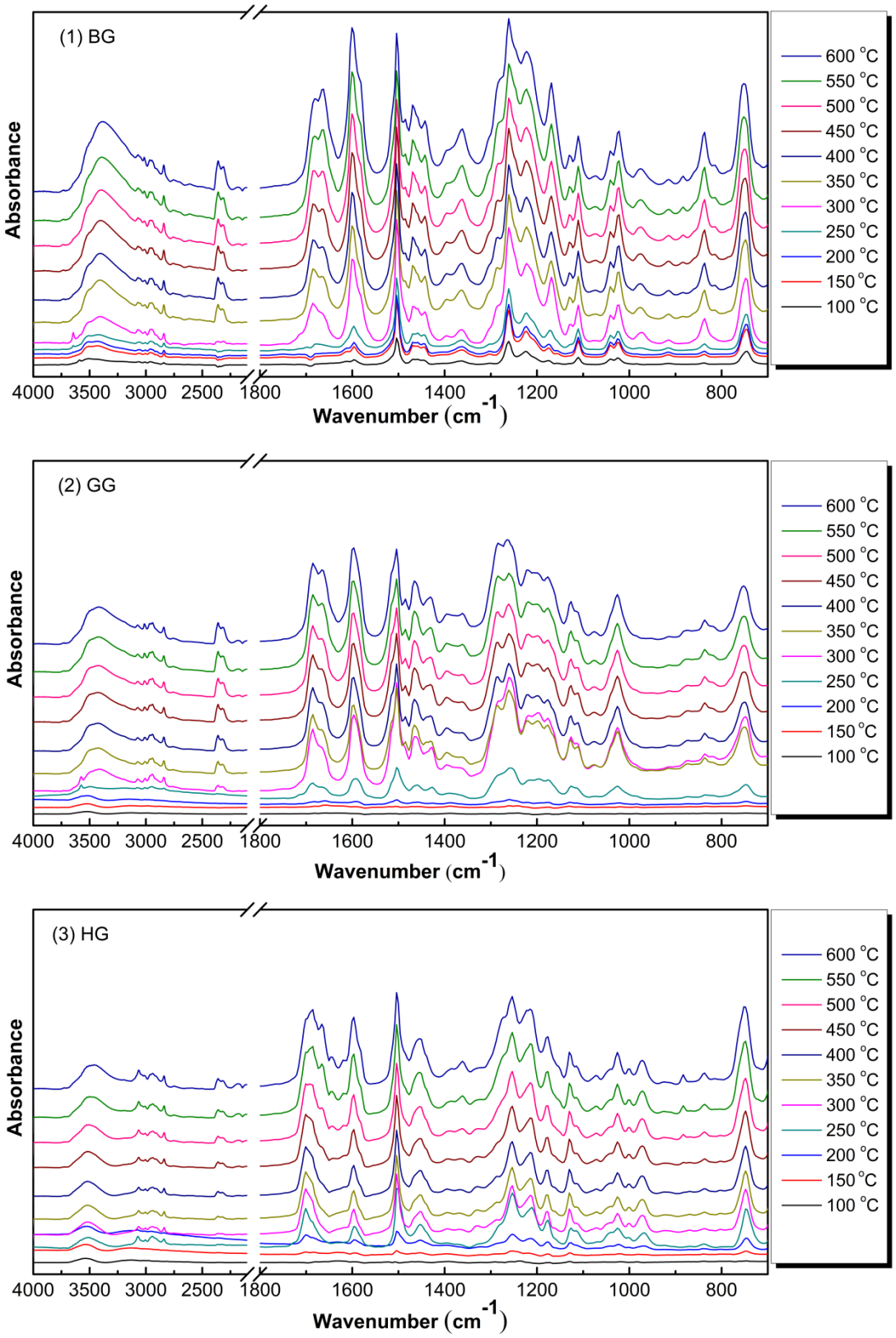

Fig. S2. The real-time monitoring results of volatiles

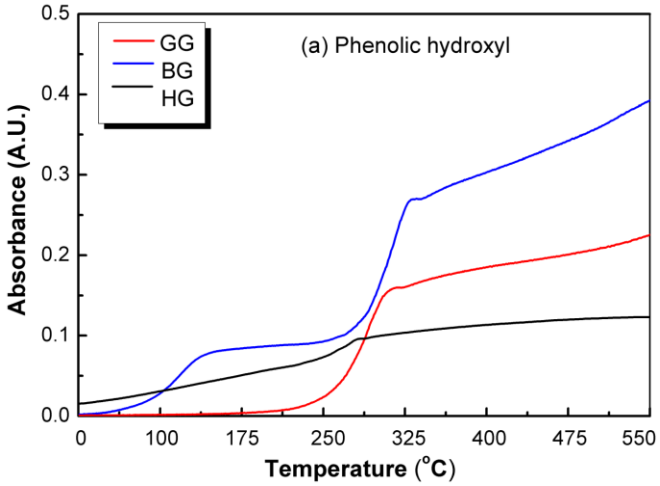
(a) Phenolic hydroxyl
GG
BG
HG
Absorbance (A.U.)
Temperature (°C)

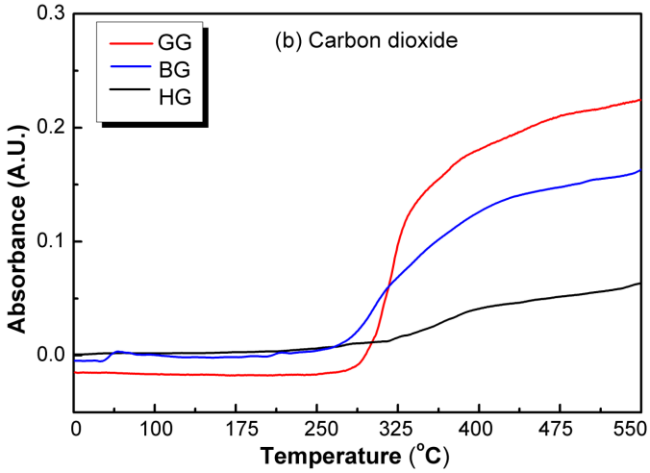
(b) Carbon dioxide
GG
BG
HG
Absorbance (A.U.)
Temperature (°C)

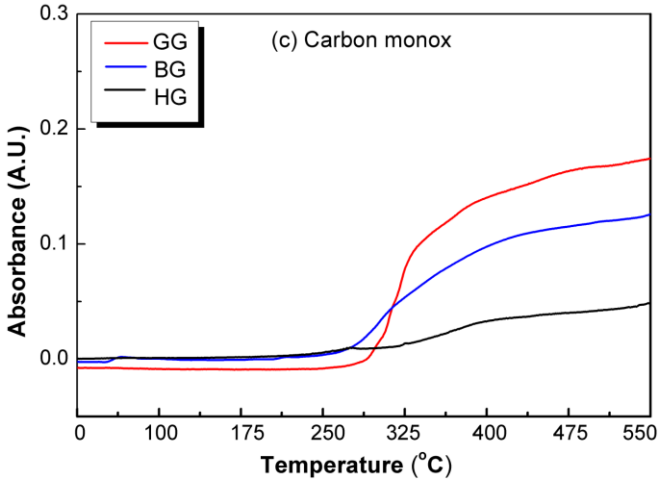
(c) Carbon monox
GG
BG
HG
Absorbance (A.U.)
Temperature (°C)

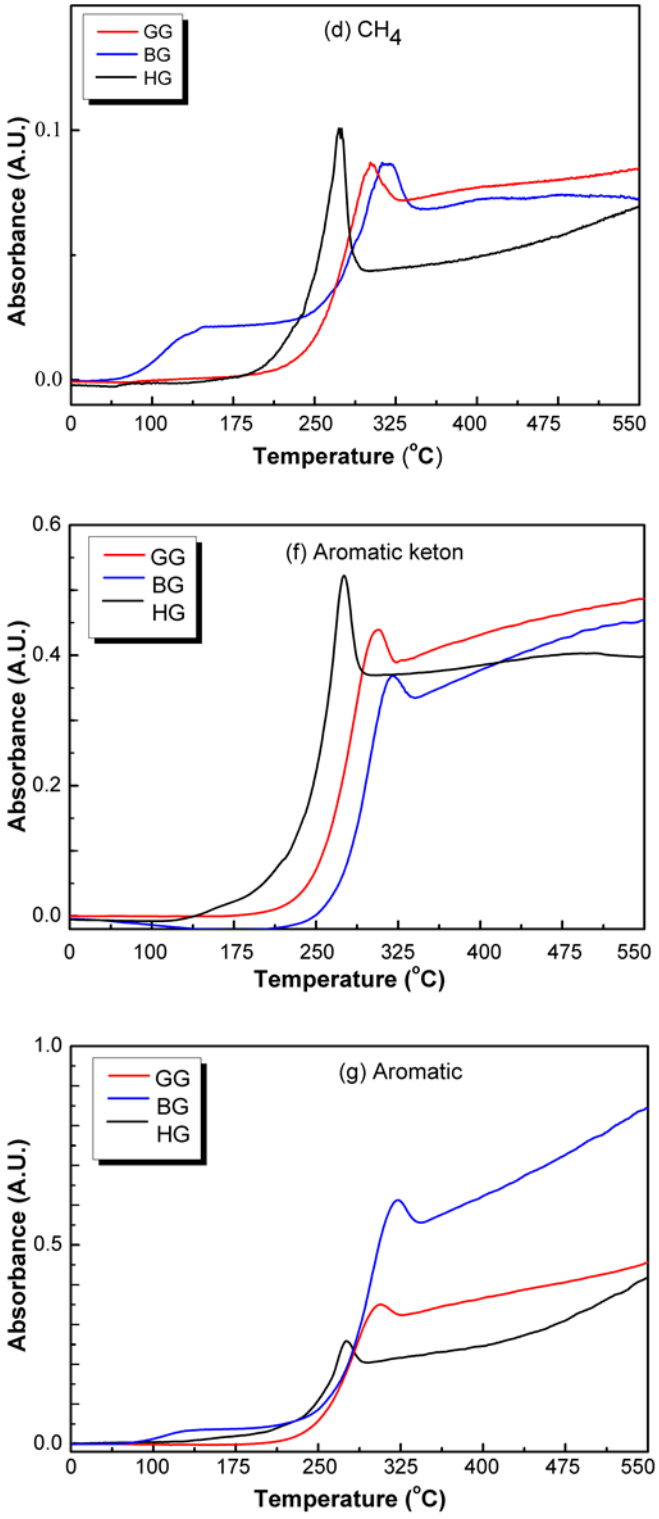

Fig. S3. Temperature-dependent relative intensities of three samples. Time resolution is 1.93 s.

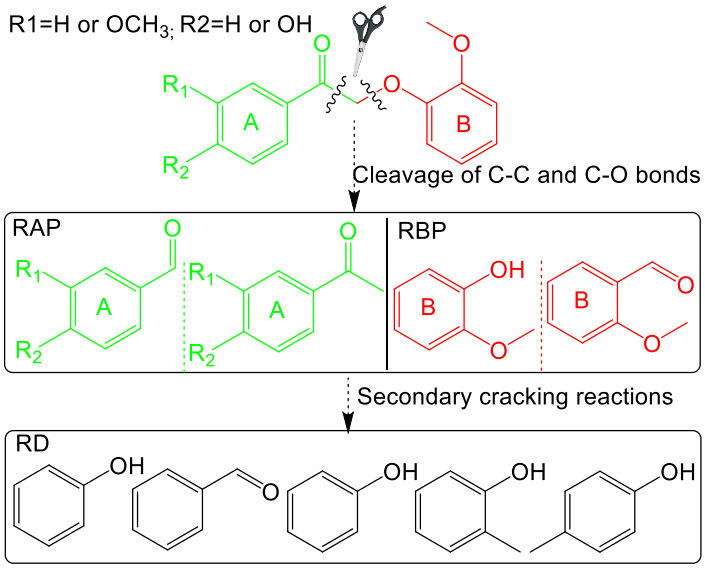

Fig. S4. Primary products (RAP and RBP) and the secondary products (RD).

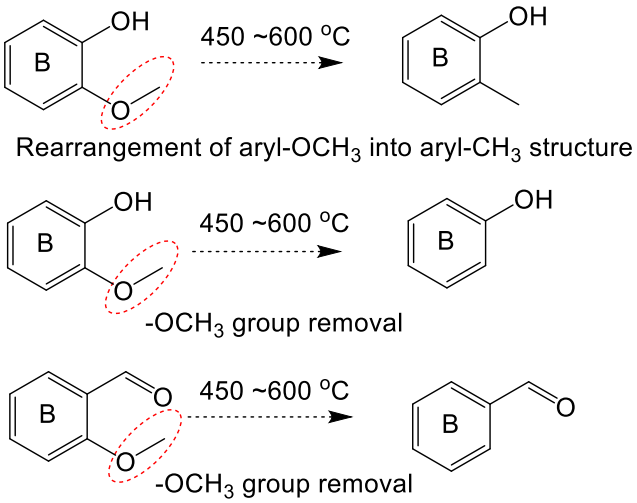

Fig. S5. A schematic diagram of the proposed mechanism of guaiacol and 2-methoxy-benzaldehyde